Dalton Transactions

ROYAL SOCIETY OF CHEMISTRY

PAPER

View Article Online
View Journal

Cite this: DOI: 10.1039/d5dt01603g

Redefining platinum(IV) chemotherapy: α-tocopherol succinate functionalization and nanoparticle encapsulation to improve cisplatin- and oxaliplatin-based therapies

Carlo Marotta, [a] Damiano Cirri, [b] Maria Chiara Maimone, [b] Chiara Giacomelli, [a] Maria Letizia Trincavelli, [a] Luca Salassa, [c,d,e] Chiara Gabbiani *[b] and Alessandro Pratesi *[b]

Platinum(IV) prodrugs offer a promising strategy to overcome the limitations of cisplatin and oxaliplatin, including systemic toxicity and acquired resistance. In this study, two novel α-tocopherol succinate-functionalized Pt(IV) complexes, [Pt(oxalato)(DACH)(OAc)(α-TOS)] (**4**) and [$PtCl_2(NH_3)_2$(OAc)(α-TOS)] (**5**), were synthesized and characterized to enhance the efficacy and selectivity of platinum-based chemotherapy. Functionalization with α-TOS (**3**) was designed to increase lipophilicity and enable selective intracellular reduction. Physicochemical characterization confirmed the chemical stability in aqueous solution and favorable lipophilicity (log $P_{o/w}$) of both complexes. Photoreduction studies demonstrated their efficient activation under biologically relevant conditions, leading to the release of active Pt(II) species and α-TOS. To enhance their pharmacokinetics and tumor selectivity, both prodrugs were encapsulated in biocompatible poly(lactic-*co*-glycolic acid)-polyethylene glycol (PLGA-PEG) nanoparticles, improving aqueous solubility and cellular uptake. Cytotoxicity assays in multiple cancer cell lines revealed that the nanoparticle formulations were generally more effective in exerting long-term cytotoxic activity compared to free cisplatin and oxaliplatin. These findings highlight the potential of α-TOS-functionalized Pt(IV) prodrugs as next-generation anticancer agents. The combination of strategic ligand modification and nanomedicine-based delivery provides a promising approach for improving the therapeutic profile of platinum-based chemotherapy.

Received 8th July 2025,
Accepted 6th August 2025

DOI: 10.1039/d5dt01603g

rsc.li/dalton

Introduction

Despite the significant advances made in anticancer therapies, there is still an urgent demand for novel drugs capable of overcoming the limitations associated with traditional chemotherapy, particularly those associated with Pt(II)-based drugs such as cisplatin (**1**) and oxaliplatin (**2**) (Scheme 1). Although these drugs have played a pivotal role in the treatment of many types of cancer, they suffer from considerable drawbacks, including severe side effects and the development of resistance phenomena by cancer cells, both of which concur in limiting their clinical applicability and efficacy.[1–5] Consequently, considerable efforts have been devoted to the development of alternative therapeutic strategies, among which Pt(IV) prodrugs represent a promising line of research. Indeed, Pt(IV) complexes offer important advantages with respect to Pt(II) drugs such as improved kinetic inertness and better selectivity for cancer cells, which results in reduced off-target reactions and may potentially allow patients to have a better clinical outcomes.[6–15] Furthermore, due to their octahedral geometry, Pt(IV) complexes can be easily axially functionalized with other bioactive molecules, potentially enhancing the overall pharmacological activity compared to their Pt(II) precursors.[6–8,11,13–22] For instance, a recently reported complex combining compound **2** and gemcitabine, two molecules administered in combination in the GEMOX clinical protocol, exemplifies this strategic enhancement of therapeutic potential.[23–25] Comprehensive reviews and research papers highlighting the mechanistic understanding and recent advancements in this field further underline the considerable yet largely unexplored potential of these Pt(IV)-based anticancer compounds.[2,26]

[a]*Department of Pharmacy, University of Pisa, Pisa, Italy*
[b]*Department of Chemistry and Industrial Chemistry, University of Pisa, Pisa, Italy. E-mail: alessandro.pratesi@unipi.it, chiara.gabbiani@unipi.it*
[c]*Donostia International Physics Center (DIPC), Donostia-San Sebastián, Euskadi, Spain*
[d]*Polimero eta Material Aurreratuak: Fisika, Kimika eta Teknologia, Kimika Fakultatea, Euskal Herriko Unibertsitatea UPV/EHU, Donostia-San Sebastián, Spain*
[e]*Ikerbasque, Basque Foundation for Science, Bilbao 48011, Spain*

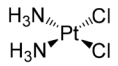

1

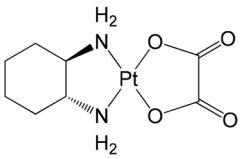

2

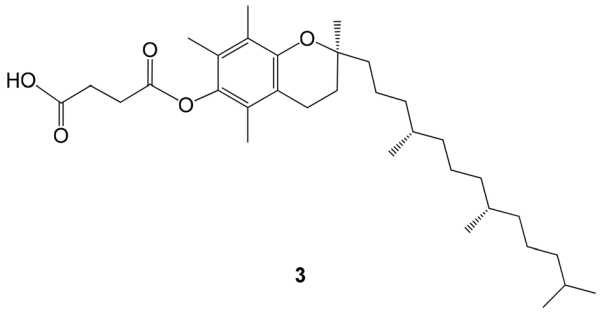

3

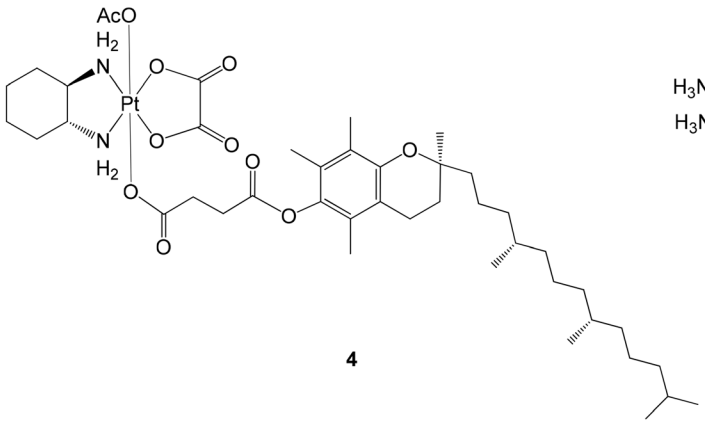

4

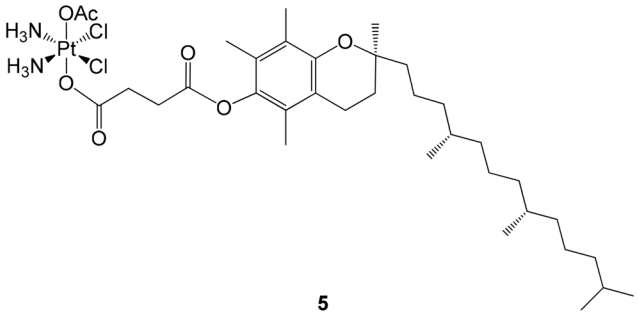

5

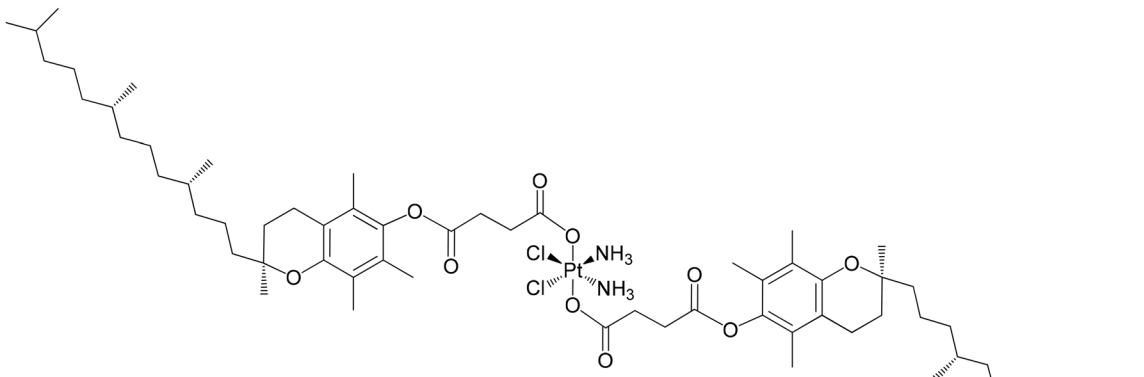

6

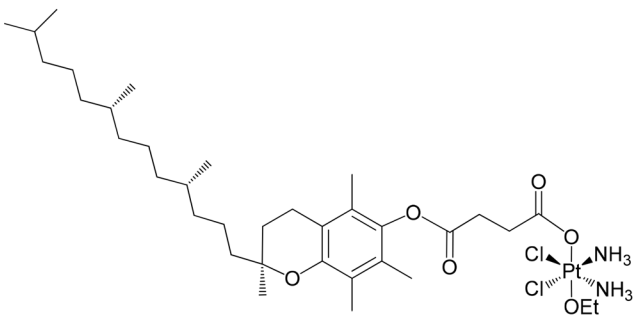

7

Scheme 1 Molecular structures of compounds **1–7**.

In this frame, an emerging concept is represented by dual-targeting complexes, which can simultaneously interfere with multiple biological pathways, such as DNA and mitochondria. Indeed, DNA is recognized as the main target of established Pt(II) chemotherapeutics, which form adducts with its purine bases, ultimately leading to cancer cell apoptosis.[27–33]

In parallel, mitochondria have gained increasing attention as crucial cellular targets due to their involvement in several key processes, such as energy metabolism, cellular growth and division, apoptosis and cancer progression.[34–40] Within this context, α-tocopherol succinate (α-TOS, **3**) (Scheme 1), an analogue of vitamin E, represents an interesting compound capable of inhibiting the mitochondrial respiratory chain.[41–44]

Interestingly, the selectivity of this molecule for cancer cells over normal cells – which have higher esterase levels capable of hydrolysing compound **3** to vitamin E – offers an additional therapeutic advantage.[45–54] Moreover, its combination with Pt drugs could also have a beneficial influence on the overall safety profile because compound **3** has shown protective effects on HEI-OC1 (House Ear Institute-Organ of Corti 1) auditory cells against cisplatin-induced cytotoxic effects.[55] Moreover, compound **3** was also shown to enhance the anticancer activity of cisplatin.[56]

Building upon the evidence that mono-functionalized α-TOS-bearing Pt(IV) complexes exhibit greater cytotoxicity compared with their di-functionalized counterparts due to their higher susceptibility to intracellular reduction,[57,58] in the present work we designed two new Pt(IV) complexes based on cisplatin and oxaliplatin featuring a single α-TOS moiety in the axial position: [Pt(oxalato)(DACH)(OAc)(α-TOS)] (**4**) and [$PtCl_2(NH_3)_2$(OAc)(α-TOS)] (**5**) (Scheme 1). Furthermore, considering the poor water solubility of their parent compounds [$PtCl_2(NH_3)_2$(α-$TOS)_2$] (**6**) and [$PtCl_2(NH_3)_2$(OEt)(α-TOS)] (**7**) (Scheme 1), they were encapsulated in PLGA-PEG nanoparticles, whose biodegradability and biocompatibility make them particularly suitable for biological applications.[57,59–61] Indeed, nanoformulations facilitate the administration of poorly water-soluble Pt(IV) complexes and, more broadly, protect them from premature reduction or hydrolysis in the extracellular environment.[26,62–64] Additionally, these carriers tend to accumulate in the tumor tissue due to both the low draining capacity of the lymphatic system and the leaky tumor vessels, thereby enhancing the delivery of the encapsulated anticancer drug to cancer cells. This results in both a reduction of the side effects and an enhancement of the pharmacological efficacy.[65–68]

The following sections describe the synthesis, characterization, reduction studies, and preliminary biological evaluation of these compounds and their nanoformulations.

Results and discussion

Synthesis and characterization

Complexes **4** and **5** were synthesized following a procedure similar to that reported in the literature for related compounds.[57] In particular, the corresponding Pt(IV) precursors, each bearing a single free –OH group in the axial position ([Pt(oxalato)(DACH)(OAc)(OH)] or [$PtCl_2(NH_3)_2$(OAc)(OH)]), were prepared according to literature procedures with minor modifications and subsequently reacted with α-TOS anhydride (Scheme 2). This reaction afforded mono-functionalized Pt(IV) prodrugs that, upon reduction, release α-TOS. Following appropriate purification, the compounds were characterized by elemental analysis, NMR spectroscopy and ESI mass spectrometry. In this regard, two different chromatographic purification strategies were tested for complex **4** (silica gel and neutral alumina) in an attempt to improve the yield. However, both methods afforded the compound in comparable yields. Based on this outcome, complex **5** was purified exclusively by chromatography on silica gel.

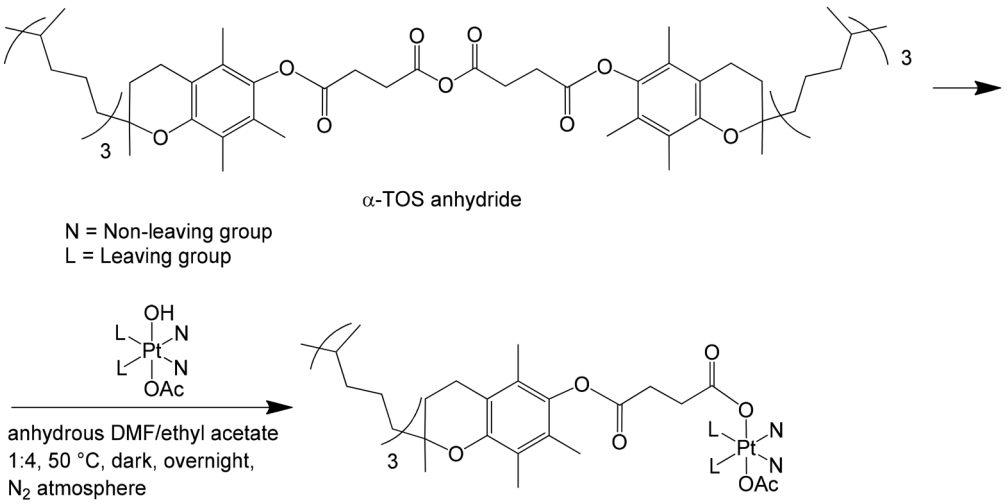

Scheme 2 Generic reaction pathway for mono-functionalized α-TOS-bearing Pt(IV) complexes.

Table 1 Log $P_{o/w}$ values for α-TOS-bearing Pt(IV) complexes

Compound	Log $P_{o/w}$ values
1[a]	−2.4
2[a]	−1.6
4	1.3
5	0.6
6[a]	1.2
7[a]	0.4

[a] Values retrieved from ref. 57 and 72.

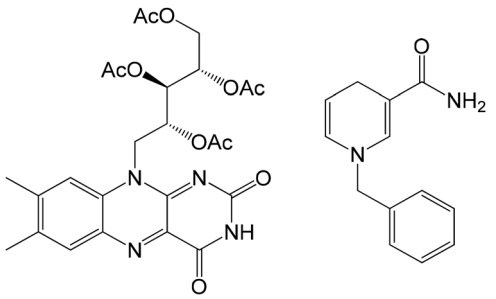

Fig. 1 Molecular structures of BNAH and TARF.

Stability in aqueous solution

The literature reports cases of Pt(IV) complexes undergoing early reduction during their hematic circulation, which results in a decrease in their efficacy as prodrugs. Indeed, tetraplatin (ormaplatin) is one of the few Pt(IV) complexes that entered clinical trials and it was found to suffer from this issue.[2,17,69] To clarify whether complexes **4** and **5** were affected by similar issues, their stability in aqueous solution was investigated. Stock solutions of these complexes were prepared in DMSO and subsequently diluted to ~5×10^{-5} M with 50 mM phosphate buffer (pH 7.4) and the electronic spectra were recorded at room temperature for 48 h. As can be seen in Fig. S1, neither of the two complexes showed any significant changes in their spectral bands over the experimental time. Therefore, sufficient stability in the aqueous buffer can be inferred for both compounds.

Water solubility and lipophilicity assessment (log $P_{o/w}$)

The aqueous solubility of complexes **4** and **5** was evaluated through quantitative NMR (qNMR) in D_2O using ethylene carbonate as an internal standard (Fig. S7 and S8). The absence of signals attributable to the complexes in the recorded

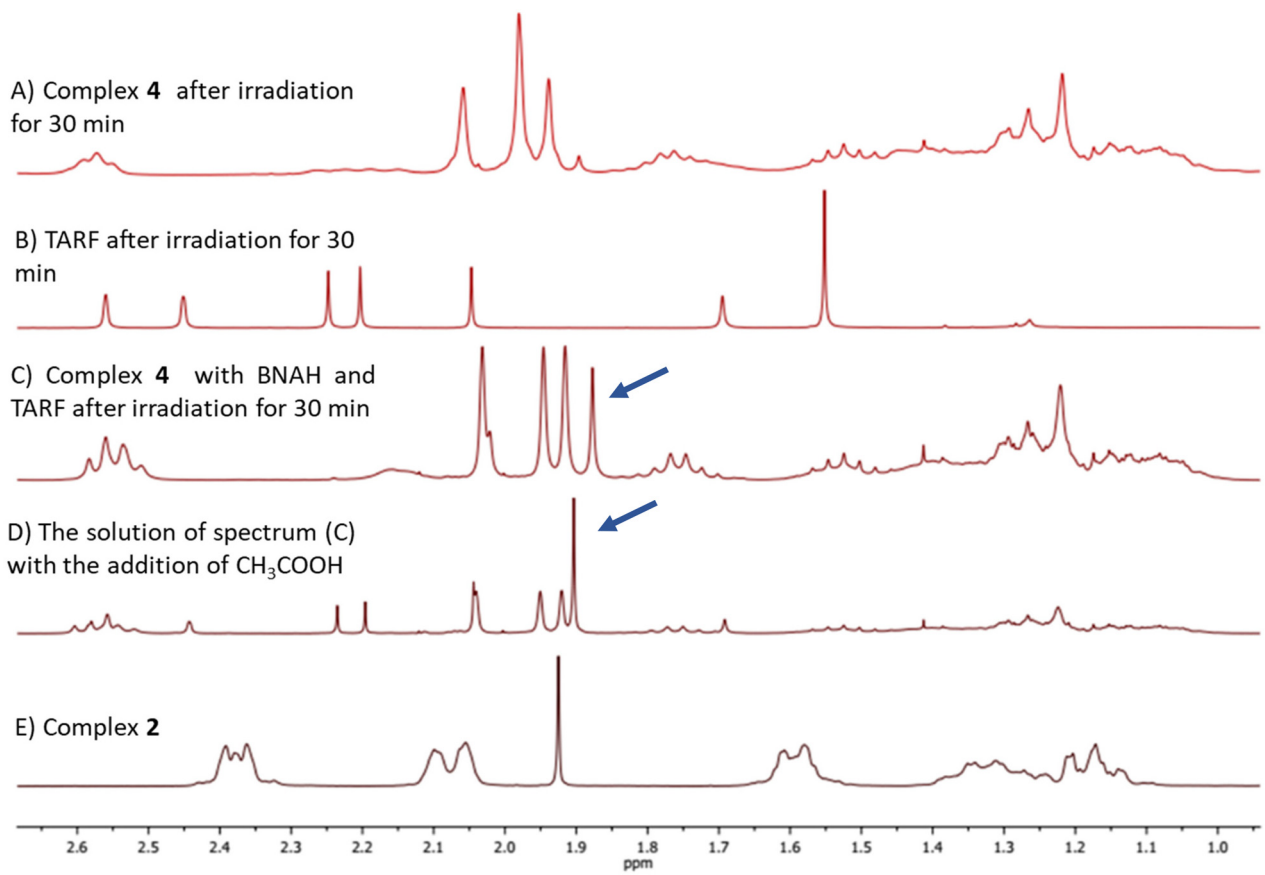

Fig. 2 ^{1}H NMR spectra (300 MHz) of (A) complex **4** (0.013 M) after irradiation for 30 min at 365 nm in CD_2Cl_2; (B) TARF (0.003 M) after irradiation for 30 min at 365 nm in CD_2Cl_2; (C) complex **4** (0.013 M) with 4.00 eq. of BNAH and 0.25 eq. of TARF after irradiation for 30 min at 365 nm in CD_2Cl_2; (D) the solution of spectrum (C) after the addition of 1 μL of CH_3COOH and 49 μL of CD_2Cl_2; (E) complex **2** – precipitated from the solution of spectrum (C) – in D_2O. Peaks corresponding to CH_3COOH in spectra (C) and (D) are highlighted with blue arrows.

spectra clearly suggests their extremely low solubility in water. This finding is perfectly in line with previously reported data obtained for two structurally related complexes (namely, $[PtCl_2(NH_3)_2(\alpha\text{-TOS})_2]$, **6**, and $[PtCl_2(NH_3)_2(OEt)(\alpha\text{-TOS})]$, **7**, Scheme 1).[57] Thus, these results further confirm that the incorporation of the hydrophobic α-TOS moiety reduces the polarity of the final molecules while enhancing their lipophilic character.

Subsequently, the lipophilicity of the synthesized compounds was evaluated by determining their $\log P_{o/w}$ values using a modified version of the shake flask method,[70,71] as detailed in the SI. The obtained values are reported in Table 1 and closely resemble those obtained for complexes **6** and **7**, further confirming the expected lipophilicity enhancement conferred by the introduction of the α-TOS moiety.

These results suggest that the equatorial ligands exert minimal influence on the water solubility of Pt(IV) complexes when bulky and lipophilic moieties, such as **3**, occupy the axial positions. This observation is evident by comparing complexes **4** and **5**. In addition, comparing the water solubility of complexes **7** (reported in ref. 57) and **5** (Fig. S8) suggests that changing the non-bioactive axial ligand from –OEt to –OAc does not significantly affect the polarity of the final complex. Conversely, the choice of equatorial ligands markedly affects the solubility in organic solvents, as evidenced by the differences in $\log P_{o/w}$ values between complexes **4** and **5**.

Photoreduction studies

Subsequently, we investigated the susceptibility of complexes **4** and **5** to intracellular reduction under conditions designed to approximate the tumor cell environment, while acknowledging the limitations imposed by the poor aqueous solubility of these compounds. Attempts to assess the reduction of these prodrugs in presence of ascorbate or glutathione were hindered by the poor solubility of complexes **4** and **5** in water, and of the bioreductants in dichloromethane. To evaluate the capability of these derivatives to undergo biological activation, we investigated their flavin-catalyzed reduction in the presence of an NADH analogue. Previous work by some of the present authors showed that flavins and flavoproteins efficiently catalyze the activation of Pt(IV) complexes under irradiation, and in some cases, even in the dark when bioreductants such as NADH or ascorbate are present.[73–77] The catalytically active species in these reactions is the doubly-reduced flavin hydroquinone, whose generation is highly accelerated by the light-promoted oxidation of the bioreductants.[77,78] Therefore, the reduction of complexes **4** and **5** was studied in the presence of 1-benzyl-1,4-dihydronicotinamide (BNAH), employed as a simplified NADH model,[79–85] together with tetra-*O*-acetyl riboflavin (TARF), a flavin derivative soluble in organic solvents and previously employed in studies on the photoreduction of Pt(IV) complexes (Fig. 1).[77]

First, the reduction of complex **4** was studied by irradiating it for 30 min with light at 365 nm in the presence of both

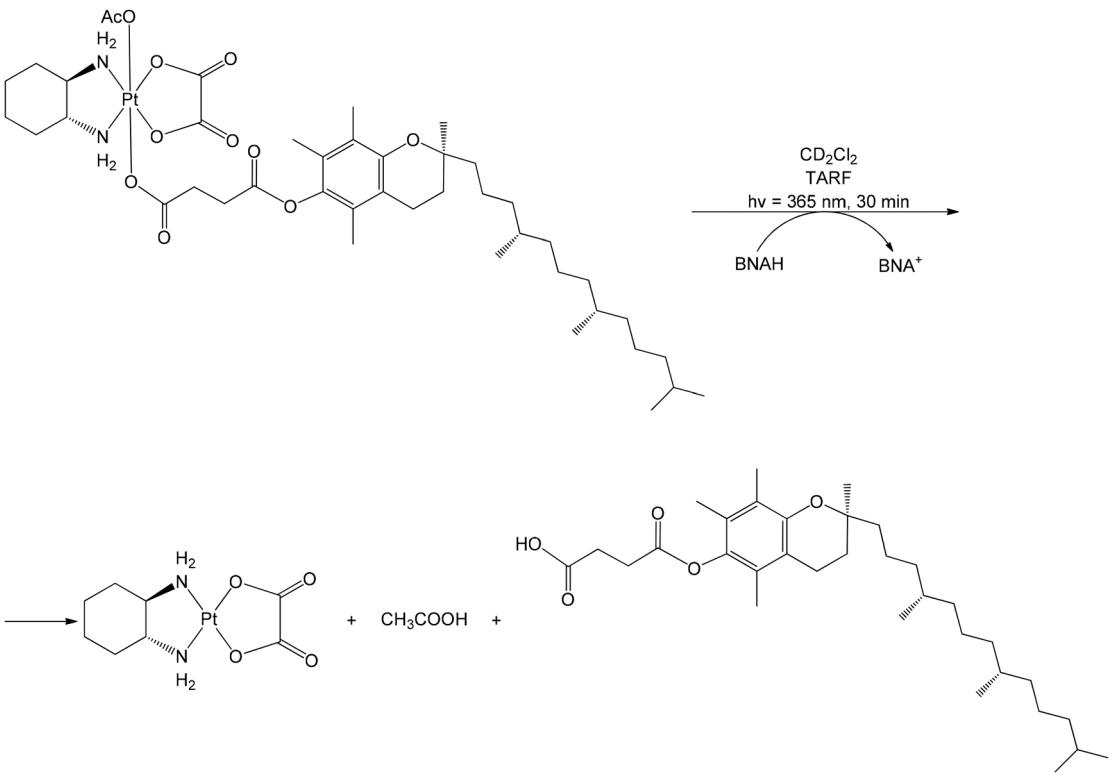

Scheme 3 Proposed mechanism for BNAH-mediated reduction.

BNAH and TARF. The resulting NMR spectrum (C, Fig. 2) showed the appearance of an additional peak at 1.88 ppm (highlighted with a blue arrow), attributable to the release of CH_3COOH. This assignment was further confirmed by spiking the NMR sample with CH_3COOH, which led to an increase in the intensity of the aforementioned signal (D, Fig. 2, the peak highlighted with a blue arrow). Moreover, during the experiment a precipitate appeared, which upon isolation and analysis was unequivocally identified as compound **2** (E, Fig. 2), thus further confirming the reductive activation of the Pt(IV) complex. In parallel, control experiments were performed by irradiating two different solutions with light at 365 nm for 30 min: one containing only complex **4** (without BNAH or TARF) and one containing only TARF (without complex **4** or BNAH). In both cases, the irradiation did not produce the formation of the signal at 1.88 ppm, thus demonstrating that this peak truly derives from the photoreduction of the studied complex and not from its decomposition or that of TARF (A and B, Fig. 2). The proposed reaction mechanism is summarized in Scheme 3. These findings suggest that complex **4** is susceptible to reductive activation under intracellular-like, biologically relevant conditions.

After confirming that complex **4** undergoes reduction upon irradiation with a high-energy wavelength (365 nm), subsequent experiments were carried out to determine whether a lower-energy, more cell-compatible wavelength (456 nm) would also be effective, and to determine whether light exposure is necessary for the reduction to occur.

In order to assess if irradiation is strictly required for the reduction process, complex **4** was dissolved in CD_2Cl_2 in the presence of BNAH and TARF, and the solution was kept in the dark for 3 h. Under these conditions, the recorded ^{1}H NMR spectrum shows the appearance of the characteristic signal at 1.88 ppm due to CH_3COOH (B, Fig. 3, the peak highlighted with a blue arrow), thus proving that the co-presence of BNAH and TARF is sufficient to induce the reduction of the complex, even without exposure to light. Subsequently, the same sample was irradiated with light at 456 nm for a total of 20 minutes, and ^{1}H NMR spectra were recorded at different time intervals. A slight yet discernible increase in the intensity of the peak ascribed to CH_3COOH was observed with increasing irradiation time (C–F, Fig. 3, peaks highlighted with blue arrows), suggesting that, although not essential, light exposure accelerates the reduction process. Additionally, as in the previous

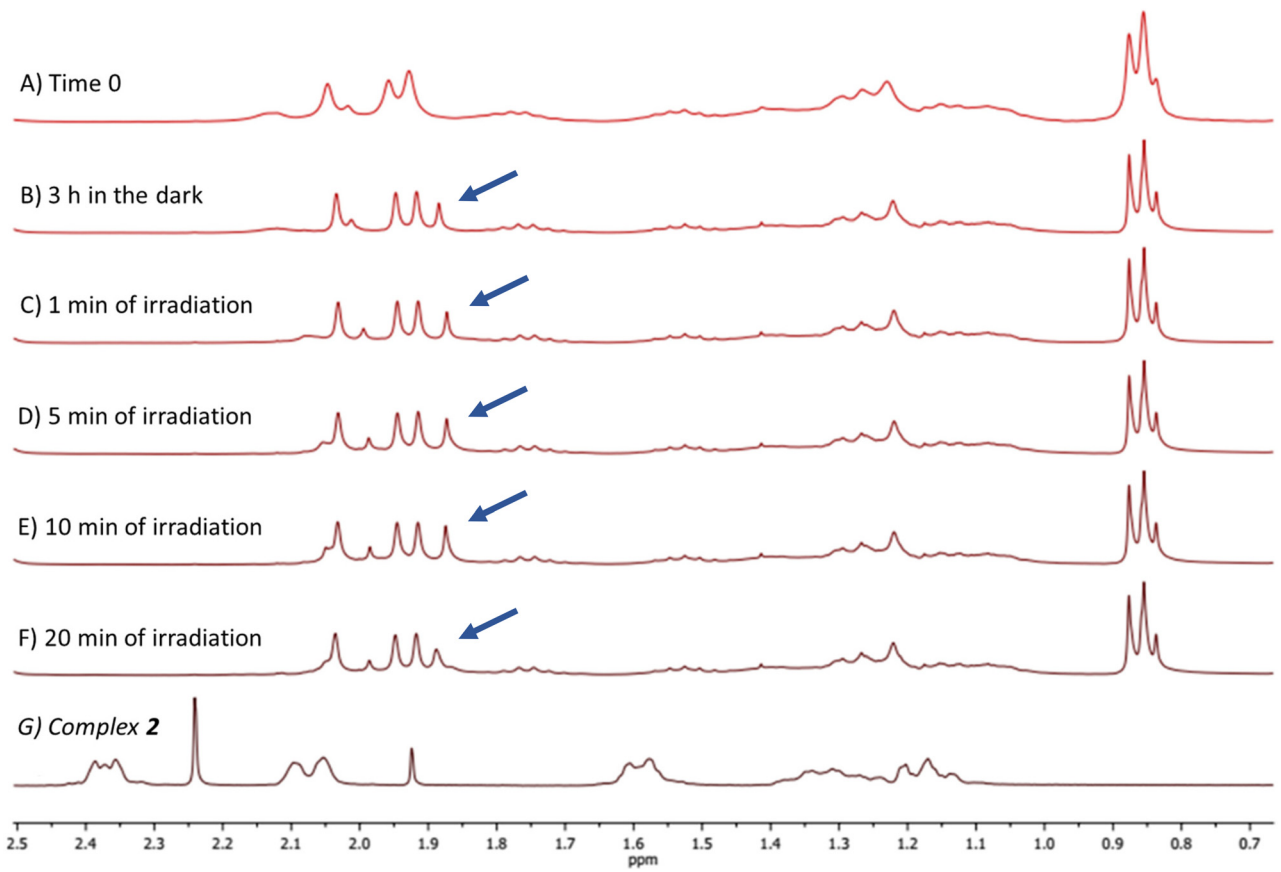

Fig. 3 ^{1}H NMR spectra (300 MHz) of complex **4** (0.013 M) with 4.00 eq. of BNAH and 0.25 eq. of TARF in CD_2Cl_2 (A) at time 0; (B) after 3 h in the dark; (C) after 1 min of irradiation at 456 nm; (D) after 5 min of irradiation at 456 nm; (E) after 10 min of irradiation at 456 nm; (F) after 20 min of irradiation at 456 nm. Finally, (G) is the ^{1}H NMR spectrum (300 MHz) of the derived complex **2** in D_2O. Peaks corresponding to CH_3COOH in spectra (B)–(F) are highlighted with blue arrows.

experiment, complex **2** precipitated from the solution following irradiation and was subsequently recovered and characterized (G, Fig. 3). Also in this case, the precipitate was identified as oxaliplatin, further confirming the reduction of complex **4**.

Furthermore, additional control studies were performed to determine whether both BNAH and TARF are required for the effective reduction of complex **4**. The results suggest that in the presence of BNAH alone, complex **4** is reduced only after irradiation with light at 456 nm, as there is no evident peak corresponding to CH_3COOH in spectrum B of Fig. 4 (in contrast to the corresponding spectrum B of Fig. 3). Conversely, a new peak around 1.9 ppm (indicative of the release of CH_3COOH) is formed after irradiation (F, Fig. 4, the peak highlighted with a blue arrow).

In addition, in a complementary experiment involving TARF alone, a small amount of complex **2** was found as a precipitate at the end of the experiment (G, Fig. 5). However, no significant peak corresponding to CH_3COOH was detected in the other spectra, possibly because its concentration was below the detection limit of the employed NMR technique (A–F, Fig. 5). Overall, these findings clearly demonstrate that the presence of both BNAH and TARF leads to a more efficient and consistent reduction of the Pt(IV) complex, likely due to their synergistic redox activity.

Given the encouraging results obtained for complex **4**, analogous experiments were carried out on complex **5** under the same experimental conditions, yielding very similar outcomes. Specifically, in the presence of BNAH alone, complex **5** is reduced only under irradiation, as evidenced by the absence of the diagnostic signal in spectrum B of Fig. S9 and its appearance in spectra C–F of the same figure (highlighted with a blue arrow). Conversely, in the presence of TARF alone, there is no evident reduction of the complex even after irradiation, as shown in spectra B–F of Fig. S10, indicating that, also in this case, TARF alone is not sufficient to promote the reduction of the complex. Notably, when both BNAH and TARF were present, the ^{1}H NMR spectrum recorded after 3 h in the dark showed an additional peak at 1.83 ppm (highlighted with a blue arrow), ascribable to CH_3COOH, confirming that the complex underwent reductive activation even in the absence of light (B, Fig. S11). These findings indicate that under the conditions employed in these experiments, complex **5** exhibits redox behavior almost superimposable to that of complex **4**, despite the different equatorial ligands.

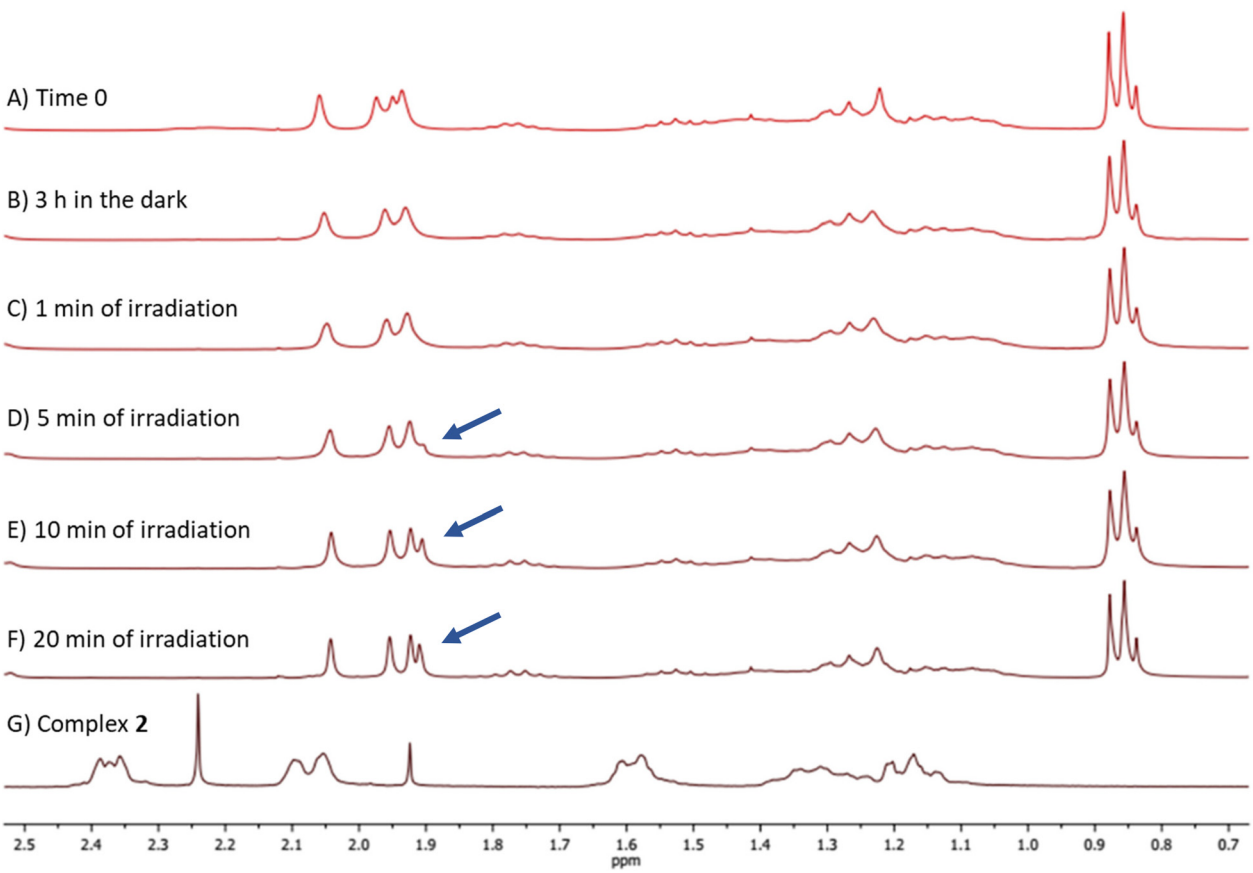

Fig. 4 ^{1}H NMR spectra (300 MHz) of complex **4** (0.013 M) with 4 eq. of BNAH (A) at time 0 in CD_2Cl_2; (B) after 3 h in the dark in CD_2Cl_2; (C) after 1 min of irradiation at 456 nm in CD_2Cl_2; (D) after 5 min of irradiation at 456 nm in CD_2Cl_2; (E) after 10 min of irradiation at 456 nm in CD_2Cl_2; (F) after 20 min of irradiation at 456 nm in CD_2Cl_2. Finally, (G) is the ^{1}H NMR spectrum (300 MHz) of the derived complex **2** in D_2O. Peaks corresponding to CH_3COOH in spectra (D)–(F) are highlighted with blue arrows.

Taken together, these results demonstrate that both Pt(IV) complexes are susceptible to reduction in the dark when BNAH and TARF are combined, mimicking conditions that may be relevant in a tumor microenvironment. Furthermore, BNAH alone is sufficient to trigger the reduction under light irradiation at 456 nm, although with slower kinetics, indicating that TARF, while not essential, enhances the efficiency of the process. This is in line with previous mechanistic studies that showed how reduced flavins are better reductants for Pt(IV) complexes than NADH derivatives.[78]

Nanoparticle preparation and evaluation of the encapsulation efficiency

To improve the pharmacological profile of the synthesized Pt (IV) complexes and address their limited aqueous solubility, the compounds were encapsulated within PLGA-PEG nanoparticles, which were chosen because of their well-known biological compatibility and suitability for drug delivery applications.[86,87]

Each nanoformulation was prepared by co-dissolving the corresponding compound and the polymeric matrix in THF. The resulting solution was added dropwise to Milli-Q water under stirring. The suspension was dialyzed against Milli-Q water to remove both the organic solvent and the unencapsulated drug. Following concentration with a rotary evaporator, the final nanoparticle formulation was obtained.

Dynamic light scattering (DLS) analysis of the empty nanoparticles – prepared using the same procedure – revealed a mean hydrodynamic diameter of 79.1 ± 1.1 nm and a polydispersity index of 0.16 ± 0.02. This size is optimal for cellular studies, as it is similar to the one obtained in a previous work involving PLGA-PEG nanoparticles loaded with another Pt(IV) complex.[24]

The encapsulation efficiency (EE) of the complexes in the nanoparticles was quantified by ICP-OES, yielding 58.3% for complex **4** and 69.3% for complex **5**, respectively. The EE of compound **3** (whose loaded nanoparticles were prepared using the aforementioned procedure) was determined using UV-Vis spectroscopy and found to be 67.3%. The concentration of the compounds within the nanoparticles employed in cellular studies was, respectively, 3090 μM for **3**, 800 μM for **4** and 1190 μM for **5**.

The cytotoxic properties of the nano-formulations of compounds **3**, **4**, and **5** were evaluated in selected cancer cell lines and compared to those of the corresponding non-encapsulated Pt(II) drugs, namely compounds **1** and **2**.

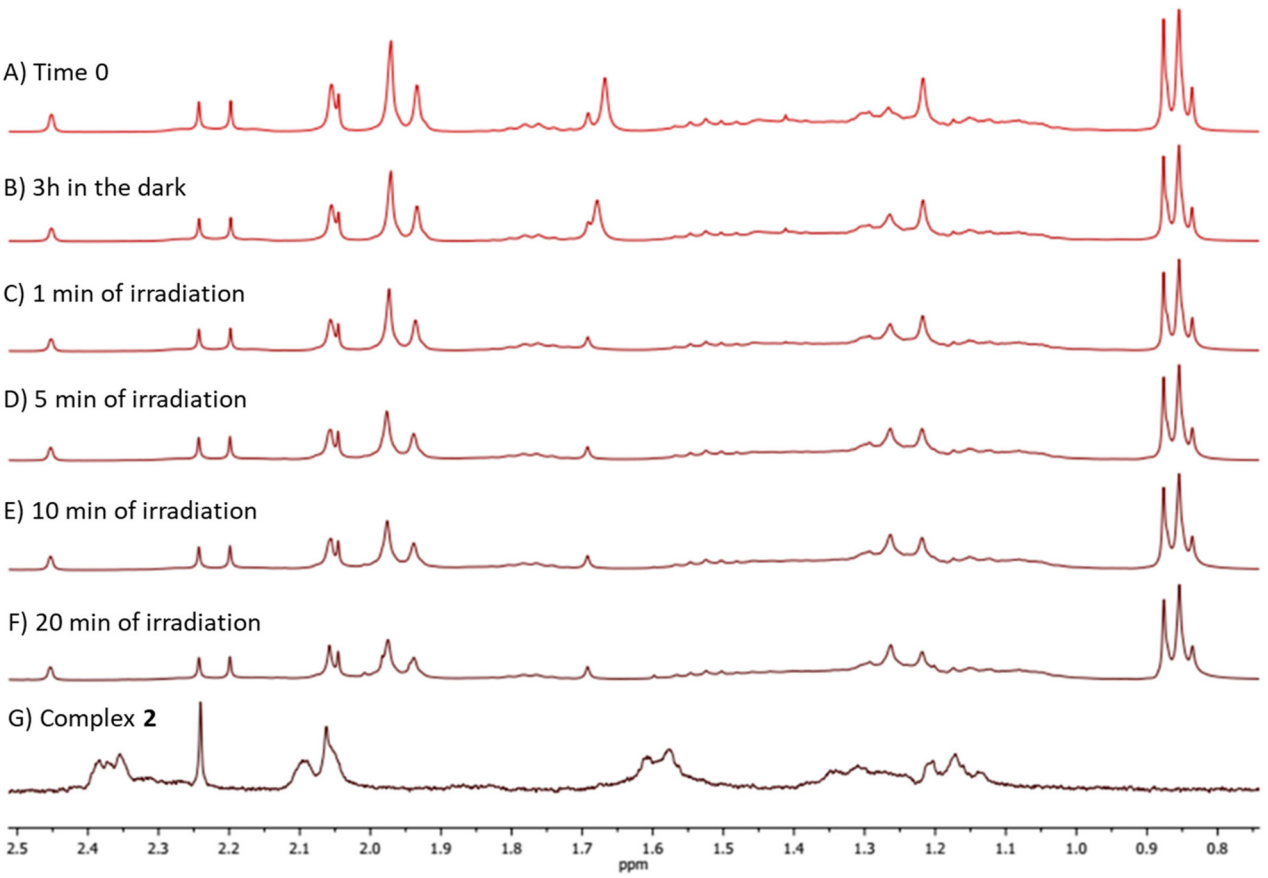

Fig. 5 ^{1}H NMR spectra (300 MHz) of complex **4** (0.013 M) with 0.25 eq. of TARF (A) at time 0 in CD_2Cl_2; (B) after 3 h in the dark in CD_2Cl_2; (C) after 1 min of irradiation at 456 nm in CD_2Cl_2; (D) after 5 min of irradiation at 456 nm in CD_2Cl_2; (E) after 10 min of irradiation at 456 nm in CD_2Cl_2; (F) after 20 min of irradiation at 456 nm in CD_2Cl_2. Finally, (G) is the ^{1}H NMR spectrum (300 MHz) of the derived complex **2** in D_2O.

Cellular studies

Cellular studies were performed on a panel of cancer cell lines, including A549 (human lung carcinoma epithelial cells), HCT116 (human colorectal carcinoma cells), MDA-MB-231 (human breast adenocarcinoma), and A2780 (human ovarian cancer cell line).

The nanoparticles *per se* were not toxic up to 72 h of treatment (Fig. S2). The antiproliferative activity of compounds **1** and **2** and of the nanoparticles loaded with compounds **3**, **4**, and **5** – hereafter abbreviated as NP-**3**, NP-**4**, and NP-**5**, respectively – was evaluated at 24 h and 72 h post-treatment (Fig. S3–S6 and Fig. 6).

In general, after 24 h, both NP-**4** and NP-**5** exhibited comparable effects on cell proliferation to those of their corresponding Pt(II) precursors and NP-**3**. Only NP-**5** in HCT116 and NP-**4** in MDA-MB231 exhibited a higher IC_{50} value. However, after 72 h, they significantly outperformed both their corresponding Pt(II) precursor and NP-**3** in reducing cell proliferation across almost all cell lines. This time-dependent increase in biological activity is consistent with the behavior of DNA-targeting agents, whose effects often become more pronounced after prolonged exposure. The activity observed after 24 h of treatment reflects direct cellular damage exerted by the compounds, whereas the one observed after 72 h of treatment may result from the activation of apoptosis and other programmed cell-death pathways. This hypothesis is consistent with the known mechanism of action of compound **3**, which induces mitochondria-mediated apoptosis, and supports the behavior of these Pt(IV) complexes as classical prodrugs which, after reduction, release the corresponding bioactive molecules.

In addition, the lower cytotoxicity observed after 24 h of treatment with NP-**4** compared to NP-**5** (Fig. S3–S6 and Fig. 6) may stem from the intrinsic reduction-resistance of tetracarboxylato-based Pt(IV) scaffolds, which are known for their relatively low reactivity toward reduction.[88–91] In contrast, NP-**5**, which is

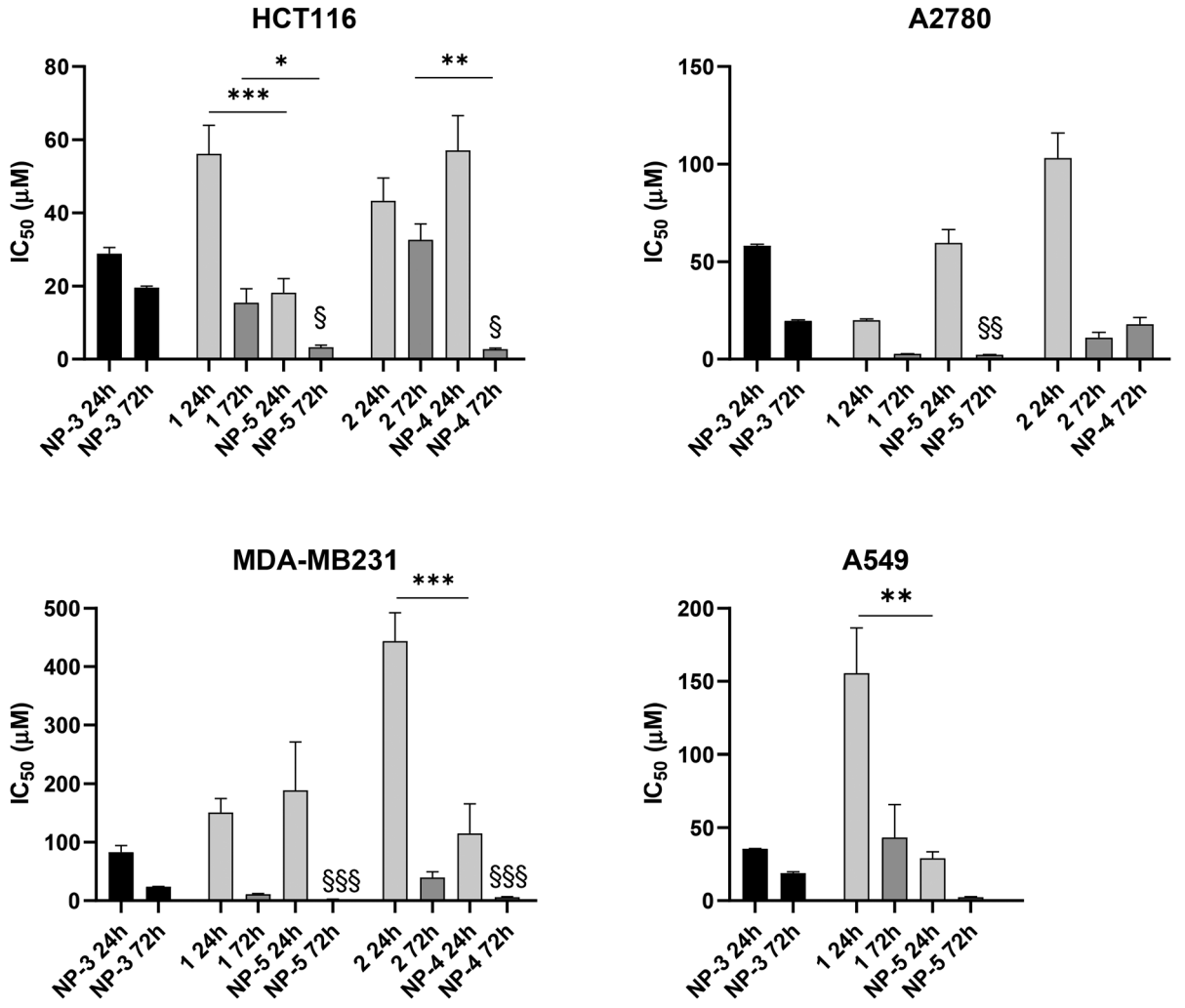

Fig. 6 IC_{50} values of the nanoformulations and of the non-encapsulated compounds on selected cancer cell lines after 24 h and 72 h of incubation. Data are presented as mean ± SEM of at least two independent experiments. The statistical significance of the differences was determined with one-way ANOVA with Bonferroni's post-test: *p < 0.05, **p < 0.01, ***p < 0.001; §p < 0.05, §§p < 0.01, and §§§p < 0.001 *vs.* respective NP-.

based on a Pt(IV) complex with two chloride ligands in the equatorial plane, displayed greater efficacy after 24 h of treatment than NP-**4**, likely due to its higher propensity for intracellular reduction and faster activation kinetics (Fig. S3–S6 and Fig. 6).

Overall, these experiments confirm that PLGA-PEG nanoparticles loaded with α-TOS-functionalized Pt(IV) complexes exhibit superior long-term cytotoxicity (72 h) compared to conventional Pt(II) drugs and α-TOS-loaded nanoparticles, especially in colorectal cancer cells. The difference in activity observed between 24 h and 72 h further highlights the importance of reduction kinetics in the mechanism of action of these dual-targeting prodrugs.

Conclusions

This work aimed to develop novel Pt(IV)-based anticancer prodrug candidates to address the key limitations of conventional platinum chemotherapy, including drug resistance and dose-limiting side effects. In this context, two mono-functionalized Pt(IV) complexes, structurally derived from clinically approved Pt(II) drugs and functionalized with compound **3** in one axial position, were synthesized and characterized through NMR spectroscopy, mass spectrometry and elemental analysis. The physicochemical properties of the complexes were investigated by assessing their stability in aqueous solution, their water-solubility and their log $P_{o/w}$ values, which provided some valuable insights into the role of axial and equatorial ligands in modulating the pharmacological properties of the final compounds. UV-Vis spectroscopy studies confirmed their sufficient stability under physiological conditions, supporting their suitability as potential prodrugs.

Photo-reduction experiments using biomimetic reducing agents demonstrated that these complexes can be reduced to their active Pt(II) counterparts – with concomitant release of the bioactive axial ligands – under conditions mimicking the tumor microenvironment. Notably, in the presence of both BNAH and TARF, reduction occurred even in the absence of light, as confirmed by cellular studies showing anticancer activity without irradiation. However, light irradiation at 456 nm, biocompatible and clinically relevant, was found to accelerate this reduction process. It is worth noting that BNAH is able to trigger Pt(IV) → Pt(II) reduction upon irradiation with light at 456 nm, but not in the dark, thereby opening the way to a convenient and selective activation of the prodrug. Finally, to overcome the water solubility issues of these molecules and enhance their biological performance, they were encapsulated in PLGA-PEG nanoparticles. *In vitro* cytotoxicity studies against a panel of human cancer cell lines revealed that the nanoparticle formulations of the α-TOS-bearing Pt(IV) complexes were generally more effective in inhibiting cell proliferation after 72 hours of treatment compared to both α-TOS-loaded nanoparticles and their corresponding Pt(II) counterparts. The difference in biological activity observed between 24 h and 72 h of treatment was attributed to the involvement of different cellular death mechanisms.

Although these results are preliminary, they highlight the promising therapeutic potential of these dual-targeting Pt(IV) prodrugs. Further studies, including deeper mechanistic studies and *in vivo* evaluations, are needed to fully characterize the true potential of these compounds. In particular, the use of 456 nm light for localized and controlled activation of complex **4** represents a compelling avenue for future research in photochemically enhanced chemotherapy.

Experimental section

Materials and methods

All solvents and chemical compounds were bought either from Sigma-Aldrich or TCI Chemicals and they were employed without further purification unless stated otherwise. Deuterated solvents were bought from Deutero (**https://www.deutero.de/**).

Milli-Q water was obtained using an "AriumPro SARTORIUS" instrument.

NMR spectra were recorded at room temperature (25 ± 2 °C) in solvents with a deuteration degree of 99.8% using either a JEOL 400 or 500 or a Bruker Fourier™ 300 NMR spectrometer. The spectra were processed using either JEOL Delta or Mestrenova (MestReNova v6.0.2-5475, MestreLab Research S. L.) software. The chemical shifts (δ) of the NMR spectra were expressed in parts per million (ppm). The spectra were calibrated on the residual signal of the solvent.[92]

High-resolution mass spectra were recorded using a TripleTOF® 5600^+ mass spectrometer (Sciex, Framingham, MA, USA) equipped with a DuoSpray® interface operating with an ESI probe. For acquisition, Analyst TF software 1.7.1 (Sciex) was used.

Elemental analyses were performed using a vario MICRO cube instrument (Elementar, Germany).

UV-Vis spectra were recorded at room temperature on an Agilent Cary 60 spectrophotometer using quartz cuvettes of 1 cm path length. The spectra were processed using Scanning Kinetics software.

The dimensions of the nanoparticles were determined using DLS. Specifically, empty nanoparticles were analyzed at room temperature using a Beckman Coulter Delsa Nano C particle analyzer (Brea, CA, USA), with nine consecutive measurements performed on the same batch.

Synthesis

Complexes **1** and **2** were synthesized according to literature-reported procedures.[93,94] $[PtCl_2(NH_3)_2(OH)(OAc)]$ was synthesized following literature-reported procedures with some minor modifications.[94–98] [Pt(oxalato)(DACH)(OH)(OAc)] was synthesized by adapting a procedure reported in the literature for the synthesis of the complex $[PtCl_2(NH_3)_2(OH)(OAc)]$ with some slight modifications.[96] The PLGA-PEG-COOH polymeric matrix was prepared according to a literature-reported procedure.[63] Compound **3** was either bought from TCI Chemicals or synthesized following a procedure reported in the literature

with some minor modifications.[99] α-TOS anhydride was synthesized as described in ref. 57.

Synthesis of complex 4. α-TOS anhydride (0.7 mL, anhydrous stock solution in *n*-hexane 1.2 M, 0.8 mmol, 0.9 g, 2 eq.) was put under nitrogen in a previously anhydrified round-bottom flask. Subsequently, the solvent (*n*-hexane) was evaporated under reduced pressure. A yellowish oil was obtained, to which [Pt(oxalato)(DACH)(OH)(OAc)] (0.162 g, 0.342 mmol) and 21 mL of a mixture of anhydrous DMF/anhydrous ethyl acetate 1 : 4 v/v were added under nitrogen. The round-bottom flask was covered with aluminum foil and the mixture was stirred at 50 °C overnight. The resulting mixture was filtered through Celite to remove the suspended white material. The resultant clear yellow solution was concentrated in a rotary evaporator (bath temperature 50 °C) to give a dark yellow oil. The crude product was subsequently purified with flash chromatography on silica gel. Elution was performed first with a mixture of $CHCl_3$/ethyl acetate 9 : 1 (to remove the subproducts) and finally with a mixture of ethyl acetate/MeOH 9 : 1 (to recover the desired product). The purified product was collected and dried under vacuum. Finally, 0.049 g (0.050 mmol) of the desired product were recovered (yield 15%) (Scheme 2). Final characterization was done through ^{1}H NMR, ^{13}C NMR, high-resolution mass spectrometry, and elemental analysis.

Alternative purification. Alternative purification was attempted in place of flash chromatography on silica gel to try to obtain the product in higher yield. The product was purified with flash chromatography on neutral alumina. First, to remove the subproducts, the column was eluted with ethyl acetate; then, to recover the product, a mixture of ethyl acetate/MeOH 9 : 1 was employed. The pure product was collected and dried under vacuum (yield 15%).

$C_{43}H_{70}N_2O_{11}Pt$ (986.11 g mol^{-1}): calculated (%) C 52.37, H 7.15, N 2.84; found (%) C 51.64, H 7.52, N 2.42.

^{1}H NMR (400 MHz, CD_2Cl_2): δ (ppm) 8.70 (br s, 1H NH_2), 8.14 (br s, 1H NH_2), 7.84 (br s, 1H NH_2), 7.43 (br s, 1H NH_2), 2.96–2.69 (m, 6H), 2.56 (t, 2H), 2.31–2.11 (m, 2H), 2.05 (s, 3H), 2.00–1.90 (m, 9H), 1.83–1.65 (m, 2H), 1.59–1.02 (m, 28H), 0.91–0.81 (m, 14H) (Fig. S12).

^{13}C NMR (125 MHz, CD_2Cl_2): δ (ppm) 182.17, 181.67, 172.71, 164.42, 164.24, 149.69, 140.96, 127.00, 125.47, 123.14, 117.90, 75.50, 62.56, 62.18, 40.93, 40.08, 39.74, 37.88, 37.80, 37.64, 33.18, 33.13, 32.13, 32.01, 31.49, 31.03, 30.08, 29.95, 28.38, 25.17, 24.81, 24.25, 23.97, 23.23, 22.86, 22.77, 21.41, 20.91, 19.91, 19.81, 13.23, 12.35, 11.90 (Fig. S13).

ESI-MS (*m*/*z*): 986.4664 $[M + H]^+$; 1008.4487 $[M + Na]^+$; 1024.4227 $[M + K]^+$ (Fig. S16–S18).

Synthesis of complex 5

A round-bottom flask was anhydrified and α-TOS anhydride (0.27 mL, anhydrous stock solution in *n*-hexane 1.2 M, 0.32 mmol, 0.33 g, 2.3 eq.) was put in it under nitrogen. Then, $[PtCl_2(NH_3)_2(OH)(OAc)]$ (0.0515 g, 0.137 mmol) and 8.2 mL of a mixture of anhydrous DMF/anhydrous ethyl acetate 1 : 4 v/v were added under nitrogen. Aluminum foil was used to cover the round-bottom flask and the mixture was stirred at 50 °C overnight. The resulting mixture was filtered through Celite to remove the suspended material, thus obtaining a yellow solution. Then, a rotary evaporator was used to concentrate the mixture (bath temperature 35 °C) until approximately 1 mL of a yellowish oil remained (0.493 g). The crude product was then purified by column chromatography on silica gel eluting, in order, with $CHCl_3$, ethyl acetate and a mixture of ethyl acetate/MeOH 9 : 1. Finally, 0.0787 g (0.0885 mmol) of the desired product were recovered as a yellowish-white solid and dried under vacuum (yield 65%) (Scheme 2). Final characterization was done through ^{1}H NMR, ^{13}C NMR, high-resolution mass spectrometry, and elemental analysis.

$C_{35}H_{62}Cl_2N_2O_7Pt$ (888.87 g mol^{-1}): calculated (%) C 47.29, H 7.03, N 3.15; found (%) C 47.38, H 7.26, N 2.98.

^{1}H NMR (400 MHz, $CDCl_3$): δ (ppm) 5.86 (br s, 6 H), 2.83 (m, 4 H), 2.57 (m, 2 H), 2.02 (m, 12 H), 1.75 (m, 2 H), 1.59–1.04 (m, 24 H), 0.86 (m, 12 H) (Fig. S14).

^{13}C NMR (100 MHz, $CDCl_3$): δ (ppm) 181.67, 181.36, 149.57, 140.45, 126.88, 125.26, 123.15, 117.73, 75.29, 75.17, 39.40, 37.46, 37.43, 37.32, 36.89, 32.81, 32.75, 31.88, 31.04, 30.35, 29.96, 28.00, 24.84, 24.49, 23.38, 22.78, 22.68, 21.09, 20.60, 19.79, 19.72, 19.68, 19.65, 19.62, 13.30, 13.15, 12.99, 12.46, 12.32, 12.15, 11.89 (Fig. S15).

ESI-MS (*m*/*z*): 889.3667 $[M + H]^+$; 911.3452 $[M + Na]^+$; 926.4402 $[M + K]^+$ (Fig. S19–S21).

UV-Vis spectroscopy studies

Stability studies of complexes **4** and **5** were performed by preparing their corresponding stock solutions in DMSO and subsequently diluting a portion of them in 50 mM phosphate buffer (pH 7.4).

The concentrations of the complexes in the analyzed samples were 5.02×10^{-5} M for complex **4** and 5.01×10^{-5} M for complex **5**, respectively. For both complexes, the analyzed solutions contained 2% DMSO. The spectra were recorded at room temperature.

Log $P_{o/w}$ determination

The partition coefficient was measured using the shake flask method with some modifications.[70,71] Octanol and H_2O (distilled after Milli-Q purification) were mixed together and shaken for 72 h until saturation of both phases. Subsequently, the complex under investigation (~1 mg) was dissolved in 4 mL of a mixture of octanol : H_2O at a ratio of 1 : 1, which was then shaken for 10 min. Next, the two phases were separated by centrifugation. Then, two aliquots of 500 μL of each phase were collected and mineralized by adding 2 mL of aqua regia 50% (which was prepared using Suprapure acids and then diluting with Milli-Q water) and heating at ~90 °C overnight. The following day, 3.5 mL of Milli-Q water were added to each aliquot to reach a final volume of 6 mL. Finally, inductively coupled plasma-optical emission spectroscopy (ICP-OES) was employed to determine the Pt concentration in each aliquot. The log $P_{o/w}$ value was calculated as follows: $\log P_{o/w} = \log_{10}([\text{compound}]_{octanol}/[\text{compound}]_{water})$. Final values were reported as the mean of two determinations.

Solubility studies

The solubility in water was measured by preparing a suspension of the complex under investigation in D_2O containing ethylene carbonate as an internal standard. Subsequently, the suspension was stirred at room temperature and then centrifuged to separate the saturated supernatant, which was then analyzed through ^{1}H NMR.

Photo-reductive studies

The compounds were dissolved in CD_2Cl_2 and subsequently treated as indicated. ^{1}H NMR spectra were recorded at specified time intervals. Irradiation was performed using a light source at either λ = 365 nm or λ = 456 nm. When a precipitate formed, it was isolated by centrifugation, washed with CH_2Cl_2, dissolved in D_2O, and analyzed through ^{1}H NMR.

CH_3COOH was added in the NMR tube as follows: 2 μL of glacial CH_3COOH were added to 98 μL of CD_2Cl_2. Then, 50 μL of this solution was added to the mixture in the NMR tube.

Nanoparticle preparation and determination of the encapsulation efficiency

Nanoparticles loaded with compound **3** and with its corresponding Pt(IV) complexes were prepared using the PLGA-PEG-COOH copolymer following the method described in ref. 63 and 100 with some modifications.

The encapsulation efficiency is defined as follows:

$$\text{Encapsulation efficiency (EE)} = \frac{[\text{loaded compound}]_i}{[\text{loaded compound}]_0} \times 100$$

where $[\text{loaded compound}]_i$ represents the concentration of the encapsulated compound, while $[\text{loaded compound}]_0$ is the concentration of the complex employed in the nanoparticle preparation.

Empty nanoparticles. Empty nanoparticles were prepared by dissolving 5.1 mg of PLGA-PEG-COOH polymeric matrix in 1 mL of THF. This solution was added dropwise to 4 mL of Milli-Q water under stirring. The resulting suspension was dialyzed overnight against Milli-Q water using a membrane with a cut-off of 3500 Da. Finally, 14.5 mL of suspension were obtained. The dimension of the nanoparticles was measured using DLS by making nine consecutive measurements on the same batch.

Nanoparticles loaded with compound 3. Nanoparticles loaded with compound **3** were prepared by dissolving around 5 mg of compound **3** and around 5 mg of PLGA-PEG-COOH polymeric matrix in 1 mL of THF. The resulting solution was added dropwise to 4 mL of Milli-Q water under stirring. The resulting suspension was dialyzed against Milli-Q water for 46 hours using a membrane with a cut-off of 3500 Da. The resulting suspension was concentrated using a rotary evaporator (bath temperature = 30 °C). The final volume of the preparation used for biological studies was 2.1 mL.

Encapsulation efficiency was measured using UV-VIS spectroscopy. More in detail, nanoparticles loaded with compound **3** were lyophilized, thus obtaining a white solid which was dissolved in THF. The absorbance of the resulting solution was measured through UV-VIS spectroscopy at 288 nm (the blank measure contained the polymeric matrix to eliminate its interference) and the corresponding concentration of compound **3** was calculated through interpolation with a previously prepared calibration curve (obtained by measuring the absorbance at 288 nm of 5 different solutions of compound **3** in THF, whose concentrations ranged from 0.09 mM to 0.25 mM).

Nanoparticles loaded with α-TOS-bearing Pt(IV) complexes. Nanoparticles loaded with α-TOS-bearing Pt(IV) complexes were prepared by dissolving around 2.5 mg of the corresponding Pt(IV) prodrug and around 5 mg of PLGA-PEG-COOH polymeric matrix in 1 mL of THF. The resulting solution was added dropwise to 4 mL of Milli-Q water under stirring. The resulting suspension was dialyzed overnight against Milli-Q water using a membrane with a cut-off of 3500 Da. The resulting suspension was concentrated using a rotary evaporator (bath temperature = 30 °C). The final volumes of the nano-formulations of complex **5** and complex **4** were, respectively, 1.6 mL and 1.8 mL. Encapsulation efficiency was measured through ICP-OES.

In vitro studies

Cell culture. A2780 (human ovarian carcinoma) and HCT116 (human colorectal carcinoma) cells were kindly provided by Prof. Tania Gamberi, Department of Experimental and Clinical Biomedical Sciences "Mario Serio", University of Florence. MDA-MB-231 (human breast adenocarcinoma) cells were purchased from ECACC. A549 cells (human lung carcinoma epithelial cells, American Type Culture Collection, CCL-195) were kindly provided by Dr. R. Danesi, University of Pisa, Italy. A2780 cells were maintained in RPMI (Corning) supplemented with 10% FBS (Corning); HCT116, A549 and MDA-MB-231 were maintained in DMEM-F12 (Corning) supplemented with 10% FBS (Corning). All cell media were supplemented with 2 mM L-glutamine, 100 U mL^{-1} penicillin, and 100 μg mL^{-1} streptomycin, and maintained at 37 °C in a humidified 5% CO_2 atmosphere.

MTS assay. Cells were seeded in 96-well microplates (10000 cells per well for A2780; 5000 cells per well for HCT116, A549 and MDA-MB-231). After 24 h, the cells were treated with different concentrations ranging from 100 nM up to 300 μM of compounds **1** and **2** or nanoparticles (NPs) containing different compounds for 24 h or 72 h. Control was treated with DMSO alone to obtain a final concentration of 1% for compound **2**, or PBS for compound **1** and NP. Then, cell viability was determined using an MTS assay (CellTiter 96 AQueous One Solution Cell Proliferation Assay kit; Promega) according to the manufacturer's instructions. The absorbance values at 490 nm were measured with a Victor Wollac 2 multimode plate reader (PerkinElmer).

Statistical analysis. Data were analyzed using GraphPad Prism 6.0 (GraphPad Software Inc., San Diego, CA). The IC_{50} values were calculated using the "non-linear fit log(inhibitor) *vs.* normalized response".

Author contributions

Conceptualisation: A. P., C. Ga., D. C., L. S., and C. M.; data curation: C. M., C. Gi., L. S. and D. C.; formal analysis: C. M., C. Gi., and L. S.; funding acquisition: A. P., C. Ga., and M. L. T.; investigation: C. M., D. C., M. C. M., and C. Gi.; methodology: D. C., C. M., L. S., A. P., and C. Gi.; supervision: A. P., D. C., L. S., and C. Ga; writing – original draft: C. M., D. C., and A. P.; writing – review and editing: all authors.

Conflicts of interest

There are no conflicts to declare.

Data availability

UV-vis, NMR and ESI-MS spectra, as well as cellular studies graphs supporting this work have been included in SI.

Supplementary information is available. See DOI: **https://doi.org/10.1039/d5dt01603g**.

Acknowledgements

The research leading to these results has received funding from the European Union – NextGenerationEU through the Italian Ministry of University and Research under PNRR – M4C2-I1.3 Project PE_00000019 "HEAL ITALIA" to CG CUP 53C22001440006. The views and opinions expressed are those of the authors only and do not necessarily reflect those of the European Union or the European Commission. Neither the European Union nor the European Commission can be held responsible for them. Professor Dario Puppi (Department of Chemistry and Industrial Chemistry, University of Pisa) is acknowledged for making available the DLS for the determination of nanoparticles' dimension. DIPC was supported by the Severo Ochoa Grant CEX2024-001494-S funded by MICIU/AEI /10.13039/501100011033.

References

1 P. Heffeter, U. Jungwirth, M. Jakupec, C. Hartinger, M. Galanski, L. Elbling, M. Micksche, B. Keppler and W. Berger, *Drug Resistance Updates*, 2008, **11**, 1–16.
2 C. Marotta, E. Giorgi, F. Binacchi, D. Cirri, C. Gabbiani and A. Pratesi, *Inorg. Chim. Acta*, 2023, **548**, 121388.
3 L. Kelland, *Nat. Rev. Cancer*, 2007, **7**, 573–584.
4 C. A. Rabik and M. E. Dolan, *Cancer Treat. Rev.*, 2007, **33**, 9–23.
5 L. Galluzzi, L. Senovilla, I. Vitale, J. Michels, I. Martins, O. Kepp, M. Castedo and G. Kroemer, *Oncogene*, 2012, **31**, 1869–1883.
6 R. G. Kenny and C. J. Marmion, *Chem. Rev.*, 2019, **119**, 1058.
7 E. Wexselblatt and D. Gibson, *J. Inorg. Biochem.*, 2012, **117**, 220–229.
8 M. D. Hall, H. R. Mellor, R. Callaghan and T. W. Hambley, *J. Med. Chem.*, 2007, **50**, 3403–3411.
9 V. Pichler, J. Mayr, P. Heffeter, O. Dömötör, É.A Enyedy, G. Hermann, D. Groza, G. Köllensperger, M. Galanksi, W. Berger, B. K. Keppler and C. R. Kowol, *Chem. Commun.*, 2013, **49**, 2249–2251.
10 U. Olszewski and G. Hamilton, *Anti-Cancer Agents Med. Chem.*, 2010, **10**, 293–301.
11 M. Galanski, M. A. Jakupec and B. K. Keppler, *Curr. Med. Chem.*, 2005, **12**, 2075–2094.
12 M. D. Hall and T. W. Hambley, *Coord. Chem. Rev.*, 2002, **232**, 49–67.
13 C. Schmidt, T. Babu, H. Kostrhunova, A. Timm, U. Basu, I. Ott, V. Gandin, V. Brabec and D. Gibson, *J. Med. Chem.*, 2021, **64**, 11364–11378.
14 D. Gibson, *J. Inorg. Biochem.*, 2019, **191**, 77–84.
15 V. Venkatesh and P. J. Sadler, in *Metallo-Drugs: Development and Action of Anticancer Agents*, ed. A. Sigel, H. Sigel, E. Freisinger, R. K. O. Sigel and De Gruyter, 2018, pp. 69–108.
16 X. Han, J. Sun, Y. Wang and Z. He, *Med. Res. Rev.*, 2015, **35**, 1268–1299.
17 G. Canil, S. Braccini, T. Marzo, L. Marchetti, A. Pratesi, T. Biver, T. Funaioli, F. Chiellini, J. D. Hoeschele and C. Gabbiani, *Dalton Trans.*, 2019, **48**, 10933–10944.
18 J. Z. Zhang, P. Bonnitcha, E. Wexselblatt, A. V. Klein, Y. Najajreh, D. Gibson and T. W. Hambley, *Chem. – Eur. J.*, 2013, **19**, 1672–1676.
19 Y. Song, K. Suntharalingam, J. S. Yeung, M. Royzen and S. J. Lippard, *Bioconjugate Chem.*, 2013, **24**, 1733–1740.
20 J. L. van der Veer, A. R. Peters and J. Reedijk, *J. Inorg. Biochem.*, 1986, **26**, 137–142.
21 A. Nemirovski, I. Vinograd, K. Takrouri, A. Mijovilovich, A. Rompel and D. Gibson, *Chem. Commun.*, 2010, **46**, 1842–1844.
22 U. Jungwirth, C. R. Kowol, B. K. Keppler, C. G. Hartinger, W. Berger and P. Heffeter, *Antioxid. Redox Signaling*, 2011, **15**, 1085–1127.
23 A. Demols, M. Peeters, M. Polus, R. Marechal, F. Gay, E. Monsaert, A. Hendlisz and J. L. Van Laethem, *Br. J. Cancer*, 2006, **94**, 481–485.
24 C. Marotta, D. Cirri, I. Kanavos, L. Ronga, R. Lobinski, T. Funaioli, C. Giacomelli, E. Barresi, M. L. Trincavelli, T. Marzo and A. Pratesi, *Pharmaceutics*, 2024, **16**, 278.
25 Definition of GEMOX – NCI Dictionary of Cancer Terms – NCI, **https://www.cancer.gov/publications/dictionaries/cancer-terms/def/gemox**, (accessed July 23, 2025).
26 M. Ravera, E. Gabano, M. J. Mcglinchey and D. Osella, *Inorg. Chim. Acta*, 2019, **492**, 32–47.
27 N. J. Wheate, S. Walker, G. E. Craig and R. Oun, *Dalton Trans.*, 2010, **39**, 8113.
28 L. Kelland, *Nat. Rev. Cancer*, 2007, **7**, 573–584.
29 Z. H. Siddik, *Oncogene*, 2003, **22**, 7265–7279.
30 D. Wang and S. J. Lippard, *Nat. Rev. Drug Discovery*, 2005, **4**, 307–320.
31 T. C. Johnstone, J. J. Wilson and S. J. Lippard, *Inorg. Chem.*, 2013, **52**, 12234–12249.

32 J. J. Wilson and S. J. Lippard, *Inorg. Chem.*, 2011, **50**, 3103–3115.
33 E. Wexselblatt and D. Gibson, *J. Inorg. Biochem.*, 2012, **117**, 220–229.
34 A. Sugiura, G.-L. McLelland, E. A. Fon and H. M. McBride, *EMBO J.*, 2014, **33**, 2142–2156.
35 S. Papa and V. P. Skulachev, *Mol. Cell. Biochem.*, 1997, **174**, 305–319.
36 D. R. Green and J. C. Reed, *Science*, 1998, **281**, 1309–1312.
37 M. J. Pinkoski, N. J. Waterhouse and D. R. Green, *Curr. Dir. Autoimmun.*, 2006, **9**, 55–73.
38 R. W. Horobin, S. Trapp and V. Weissig, *J. Controlled Release*, 2007, **121**, 125–136.
39 D. D. Newmeyer and S. Ferguson-Miller, *Cell*, 2003, **112**, 481–490.
40 S. Jin, Y. Hao, Z. Zhu, N. Muhammad, Z. Zhang, K. Wang, Y. Guo, Z. Guo and X. Wang, *Inorg. Chem.*, 2018, **57**, 11135–11145.
41 G. A. S. dos Santos, R. S. Abreu E Lima, C. R. Pestana, A. S. G. Lima, P. S. Scheucher, C. H. Thomé, H. L. Gimenes-Teixeira, B. A. A. Santana-Lemos, A. R. Lucena-Araujo, F. P. Rodrigues, R. Nasr, S. A. Uyemura, R. P. Falcão, H. De Thé, P. P. Pandolfi, C. Curti and E. M. Rego, *Leukemia*, 2012, **26**, 451–460.
42 G. W. Burton and M. G. Traber, *Annu. Rev. Nutr.*, 1990, **10**, 357–382.
43 A. Azzi and A. Stocker, *Prog. Lipid Res.*, 2000, **39**, 231–255.
44 V. R. Fantin and P. Leder, *Oncogene*, 2006, **25**, 4787–4797.
45 J. Neuzil, J. C. Dyason, R. Freeman, L.-F. Dong, L. Prochazka, X.-F. Wang, I. Scheffler and S. J. Ralph, *J. Bioenerg. Biomembr.*, 2007, **39**, 65–72.
46 Y. Zhao, J. Neuzil and K. Wu, *Mol. Nutr. Food Res.*, 2009, **53**, 129–139.
47 W. Yu, B. G. Sanders and K. Kline, *Cancer Res.*, 2003, **63**, 2483–2491.
48 T. Weber, H. Dalen, L. Andera, A. Nègre-Salvayre, N. Augé, M. Sticha, A. Lloret, A. Terman, P. K. Witting, M. Higuchi, M. Plasilova, J. Zivny, N. Gellert, C. Weber and J. Neuzil, *Biochemistry*, 2003, **42**, 4277–4291.
49 X.-F. Wang, P. K. Witting, B. A. Salvatore and J. Neuzil, *Biochem. Biophys. Res. Commun.*, 2005, **326**, 282–289.
50 C.-W. Shiau, J.-W. Huang, D.-S. Wang, J.-R. Weng, C.-C. Yang, C.-H. Lin, C. Li and C.-S. Chen, *J. Biol. Chem.*, 2006, **281**, 11819–11825.
51 M. P. Malafa and L. T. Neitzel, *J. Surg. Res.*, 2000, **93**, 163–170.
52 J. Quin, D. Engle, A. Litwiller, E. Peralta, A. Grasch, T. Boley and S. Hazelrigg, *J. Surg. Res.*, 2005, **127**, 139–143.
53 J. Neuzil, *Br. J. Cancer*, 2003, **89**, 1822–1826.
54 M. P. Malafa, F. D. Fokum, J. Andoh, L. T. Neitzel, S. Bandyopadhyay, R. Zhan, M. Iiizumi, E. Furuta, E. Horvath and K. Watabe, *Int. J. Cancer*, 2006, **118**, 2441–2447.
55 S. K. Kim, G. J. Im, Y. S. An, S. H. Lee, H. H. Jung and S. Y. Park, *Int. J. Pediatr. Otorhinolaryngol*, 2016, **86**, 9–14.
56 K. N. Prasad, C. Hernandez, J. Edwards-Prasad, J. Nelson, T. Borus and W. A. Robinson, *Nutr. Cancer*, 1994, **22**, 233–245.
57 C. Marotta, D. Cirri, T. Funaioli, C. Gabbiani and A. Pratesi, *Comments Inorg. Chem.*, 2024, 1–10.
58 K. Suntharalingam, A. Y. Song and S. J. Lippard, *Chem. Commun.*, 2014, **50**, 2465–2468.
59 K. Zhang, X. Tang, J. Zhang, W. Lu, X. Lin, Y. Zhang, B. Tian, H. Yang and H. He, *J. Controlled Release*, 2014, **183**, 77–86.
60 R. A. Jain, *Biomaterials*, 2000, **21**, 2475–2490.
61 S. Fredenberg, M. Wahlgren, M. Reslow and A. Axelsson, *Int. J. Pharm.*, 2011, **415**, 34–52.
62 P. Xie, Q. Jin, Y. Li, J. Zhang, X. Kang, J. Zhu, X. Mao, P. Cao and C. Liu, *Biomater. Sci.*, 2022, **10**, 153–157.
63 A. Menconi, T. Marzo, L. Massai, A. Pratesi, M. Severi, G. Petroni, L. Antonuzzo, L. Messori, S. Pillozzi and D. Cirri, *Biometals*, 2021, **34**, 867–879.
64 N. Margiotta, S. Savino, N. Denora, C. Marzano, V. Laquintana, A. Cutrignelli, J. D. Hoeschele, V. Gandin and G. Natile, *Dalton Trans.*, 2016, **45**, 13070–13081.
65 M. Afshari, K. Derakhshandeh and L. Hosseinzadeh, *J. Microencapsulation*, 2014, **31**, 239–245.
66 P. Ebrahimnejad, R. Dinarvand, A. Sajadi, M. R. Jaafari, A. R. Nomani, E. Azizi, M. Rad-Malekshahi and F. Atyabi, *Nanomedicine*, 2010, **6**, 478–485.
67 A. Kosasih, B. J. Bowman, R. J. Wigent and C. M. Ofner 3rd, *Int. J. Pharm.*, 2000, **204**, 81–89.
68 R. Singh and J. W. J. Lillard, *Exp. Mol. Pathol.*, 2009, **86**, 215–223.
69 S. G. Chaney, G. K. Till and S. Wyrick, *Cancer Res.*, 1990, **50**, 4539–4545.
70 T. Marzo, S. Pillozzi, O. Hrabina, J. Kasparkova, V. Brabec, A. Arcangeli, G. Bartoli, M. Severi, A. Lunghi, F. Totti, C. Gabbiani, A. G. Quiroga and L. Messori, *Dalton Trans.*, 2015, **44**, 14896–14905.
71 M. V. Baker, P. J. Barnard, S. J. Berners-Price, S. K. Brayshaw, J. L. Hickey, B. W. Skelton and A. H. White, *Dalton Trans.*, 2006, 3708–3715.
72 D. Cirri, M. G. Fabbrini, A. Pratesi, L. Ciofi, L. Massai, T. Marzo and L. Messori, *Biometals*, 2019, **32**, 813–817.
73 J. Gurruchaga-Pereda, V. Martínez-Martínez, E. Formoso, O. Azpitarte, E. Rezabal, X. Lopez, A. L. Cortajarena and L. Salassa, *J. Phys. Chem. Lett.*, 2021, **12**, 4504–4508.
74 S. Alonso-de Castro, E. Ruggiero, A. Ruiz-de-Angulo, E. Rezabal, J. C. Mareque-Rivas, X. Lopez, F. López-Gallego and L. Salassa, *Chem. Sci.*, 2017, **8**, 4619–4625.
75 S. Alonso-de Castro, A. Terenzi, S. Hager, B. Englinger, A. Faraone, J. C. Martínez, M. S. Galanski, B. K. Keppler, W. Berger and L. Salassa, *Sci. Rep.*, 2018, **8**, 17198.
76 S. Alonso-de Castro, A. L. Cortajarena, F. López-Gallego and L. Salassa, *Angew. Chem., Int. Ed.*, 2018, **57**, 3143–3147.
77 J. Gurruchaga-Pereda, V. Martínez-Martínez, E. Rezabal, X. Lopez, C. Garino, F. Mancin, A. L. Cortajarena and L. Salassa, *ACS Catal.*, 2020, **10**, 187–196.
78 S. Scoditti, E. Dabbish, G. E. Pieslinger, E. Rezabal, X. Lopez, E. Sicilia and L. Salassa, *Phys. Chem. Chem. Phys.*, 2022, **24**, 5323–5329.

79 Y.-C. Liu, X.-Z. Li, C. Yang and Q.-X. Guo, *Bioorg. Chem.*, 2001, **29**, 14–18.
80 X.-Q. Zhu, J.-Y. Zhang and J.-P. Cheng, *J. Org. Chem.*, 2006, **71**, 7007–7015.
81 S. Fukuzumi, O. Inada and T. Suenobu, *J. Am. Chem. Soc.*, 2003, **125**, 4808–4816.
82 S. Fukuzumi, O. Inada and T. Suenobu, *J. Am. Chem. Soc.*, 2002, **124**, 14538–14539.
83 B. Zhang, X.-Q. Zhu, J.-Y. Lu, J. He, P. G. Wang and J.-P. Cheng, *J. Org. Chem.*, 2003, **68**, 3295–3298.
84 A. Kobayashi, H. Konno, K. Sakamoto, A. Sekine, Y. Ohashi, M. Iida and O. Ishitani, *Chem. – Eur. J.*, 2005, **11**, 4219–4226.
85 S. Fukuzumi, Y. Fujii and T. Suenobu, *J. Am. Chem. Soc.*, 2001, **123**, 10191–10199.
86 A. Kumari, S. K. Yadav and S. C. Yadav, *Colloids Surf., B*, 2010, **75**, 1–18.
87 N. Wilkosz, G. Łazarski, L. Kovacik, P. Gargas, M. Nowakowska, D. Jamróz and M. Kepczynski, *J. Phys. Chem. B*, 2018, **122**, 7080–7090.
88 Z. Wang, N. Wang, S. C. Cheng, K. Xu, Z. Deng, S. Chen, Z. Xu, K. Xie, M. K. Tse, P. Shi, H. Hirao, C. C. Ko and G. Zhu, *Chem*, 2019, **5**, 3151–3165.
89 J. Z. Zhang, E. Wexselblatt, T. W. Hambley and D. Gibson, *Chem. Commun.*, 2012, **48**, 847–849.
90 G. Thiabaud, R. McCall, G. He, J. F. Arambula, Z. H. Siddik and J. L. Sessler, *Angew. Chem., Int. Ed.*, 2016, **55**, 12626–12631.
91 H. P. Varbanov, S. M. Valiahdi, C. R. Kowol, M. A. Jakupec, M. Galanski and B. K. Keppler, *Dalton Trans.*, 2012, **41**, 14404–14415.
92 G. R. Fulmer, A. J. M. Miller, N. H. Sherden, H. E. Gottlieb, A. Nudelman, B. M. Stoltz, J. E. Bercaw and K. I. Goldberg, *Organometallics*, 2010, **29**, 2176–2179.
93 T. Marzo, A. Pratesi, D. Cirri, S. Pillozzi, G. Petroni, A. Guerri, A. Arcangeli, L. Messori and C. Gabbiani, *Inorg. Chim. Acta*, 2018, **470**, 318–324.
94 D. A. Tolan, Y. K. Abdel-Monem and M. A. El-Nagar, *Appl. Organomet. Chem.*, 2019, **33**, 1–12.
95 X. Wang, C. Yang, Y. Zhang, X. Zhen, W. Wu and X. Jiang, *Biomaterials*, 2014, **35**, 6439–6453.
96 M. Ravera, E. Gabano, S. Tinello, I. Zanellato and D. Osella, *J. Inorg. Biochem.*, 2017, **167**, 27–35.
97 Y. Dai, Y. Zhu, J. Cheng, J. Shen, H. Huang, M. Liu, Z. Chen and Y. Liu, *Chem. Commun.*, 2020, **56**, 14051–14054.
98 S. Liang, L. Han, W. Mu, D. Jiang, T. Hou, X. Yin, X. Pang, R. Yang, Y. Liu and N. Zhang, *J. Mater. Chem. B*, 2018, **6**, 7004–7014.
99 M. Gelo-Pujic, J.-R. Desmurs, S. Delaire, A. Adao and D. Tawil, *Int. J. Cosmet. Sci.*, 2008, **30**, 195–204.
100 R. Palao-Suay, L. Rodrigáñez, M. R. Aguilar, C. Sánchez-Rodríguez, F. Parra, M. Fernández, J. Parra, J. Riestra-Ayora, R. Sanz-Fernández and J. S. Román, *Macromol. Biosci.*, 2016, **16**, 395–411.